GEOLOGICAL AND CLIMATE HISTORY OF MARS: IDENTIFICATION OF POTENTIAL WARM AND WET CLIMATE 'FALSE POSITIVES'. James W. Head[1], James L. Fastook[2] and Robin D. Wordsworth[3], [1]Brown University, Providence, RI 02912 USA, [2]University of Maine, Orono, ME 04469 USA, [3]Harvard University, Cambridge, MA 02138 US, (james_head@brown.edu).

Introduction: We recently outlined a synthesis of major changes in perspectives on the geological and climate history of Mars in the last three decades (1) and explored an inverse modeling approach to the climate history to assess the factors responsible for a transition from an ancient period of higher mean annual surface temperatures (MAT) and atmosphere pressures (and the predicted dominantly altitude-dependent distribution (ADD) of snow and ice), to the significantly lower atmosphere temperatures and pressures and the bipolar dominantly latitude-dependent distribution (LDD) of snow and ice on today's Mars (2-3). On the basis of these approaches, we here revisit a forward model of Mars' geological/climate history, beginning in the Late Noachian, and assess the processes operating and how they might relate to the required decrease to the MAT (~213K) and P_{atm} (~6 mbars) observed today.

1) Early-Middle Noachian: Primary P_{atm} was higher, but unknown. Three major basins followed the huge pre-Noachian Borealis basin (4) and are together likely to have blown off a major part of the primary atmosphere (5). Noachian phyllosilicates (6) form from: 1) torrential hot rains accompanying basin formation (7) and 2) deep warm groundwater alteration later excavated by craters to the surface (8). Post-basin Middle-Late Noachian volcanism appears insufficient to generate a robust secondary atmosphere (9); ambient P_{atm} was likely equal to/less than ~500 mbar (10). In this case, MAT is very cold, well below 273K (11); the cryosphere is global, the hydrological system is horizontally stratified (12), and P_{atm} is sufficient to ensure an adiabatic cooling effect (ACE) and an icy highlands (LNIH).

2) Late Noachian: Clear evidence of significant aMounts of ice in the southern uplands (11-13), and the south circumpolar region; significant ice accumulation on the eastern Hellas rim (14-15) predicted to flow down Hellas basin wall and onto the basin floor, with associated shear heating/some meltwater generation. Apparent freezing in the globally deepest/warmest place on Mars (16) strongly suggests that the ambient climate was cold and icy (C&I). Evidence for Noachian oceans (Northern Lowlands, Hellas) highly uncertain and/or covered by younger deposit. Tharsis appears largely built by this time (17); thus likely to have been at the equator and an additional cold-trap. Very low MAT and global cryosphere disfavor equatorial rainfall and groundwater migration to produce LN Meridiani evaporites (18).

3) Noachian-Hesperian Boundary: Water inventory and glacial flow models (9,13) suggest that LNIH have relatively thin (few 100 m) ice, lying generally above a +1 km ELA. Valley networks (VN) form in highlands where ice is predicted to accumulate; drainage forms open-closed basin lakes (OBL/CBL) in slightly lower adjacent highlands (13,19-21). Duration (~10^5-10^6 a) is minimal, activity intermittent (22,10); top-down melting of a cold-based ice sheet appears increasingly likely (12); some boundary deposits (23) but no substantial drainage into the northern lowlands (NL) (24). NW Hellas rim shows evidence of altitude-dependent sublimation (low) and melting (high) (25), suggesting a rising ELA, with PDT/PST perhaps responsible for minimal glacial ice melting. LN extrusive/explosive volcanism in Malea Planum and elsewhere; P_{atm} nears released gas maximum for H_2O (~2800 ppm) and high sulfur species (~2600 ppm); may contribute acid precipitation (26).

4) Early Hesperian: Major VN/OBL/CBL rapidly decline. Significant regions of Mars (>30%) flooded by EH volcanic plains, accompanied by centralized edifice volcanism in Malea, Hesperia, Syrtis and elsewhere (9); Northern lowlands resurfaced to a depth of hundreds of meters (27). Due to widespread distribution of snow and ice (13) ample opportunity for associated volcano-ice interactions and production of significant meltwater volumes (27). Explosive volcanism and S release unlikely to be a cause of global warming (28), except locally where they can cause local melting, radial channels and lahars (29); regional tephra can melt snow/ice (thin) and preserve it from ablation (thicker)(30). Ambient climate remains C&I; global cryosphere thickens. Volcano-Ice interactions are likely to have been extremely important where volcanism encounters surface snow and ice, or where local eruptions have released sulfur compounds (high altitudes favored) and produced acid precipitation. Valles Marineris (VM) opens and deepens (17).

4) Late Hesperian: Period of formation of outflow channels (OC); commonly thought of as being due to catastrophic groundwater release and to have occurred nearly simultaneously resulting in flooding of the northern lowlands and formation of a northern lowlands ocean (31). But: 1) CSFD data suggest that OCs formed in the LN, EH and LH, and into the Amazonian (span of >1Ga) (32); 2) interpreted OC volumes vastly less than volume needed to flood to 'shoreline' contact (need 40-50 events) (9); 3) several OCs characterized by multiple episodes; 4) climate modeling of an outflow channel suggests little lasting influence on the climate system; lifetime of surface water in single OC event is hundreds of years (33). Where does the water come from? Global climate models predict that Tharsis remains a high-altitude cold trap and water inventory/glacial flow models predict ample ice accumulation and glaciation there. Multiple options for liquid water generation exist: Volcano-ice 1) contact and 2)

deferred melting (27); 3) plinian eruption column local atmospheric warming and ice melting (28); 4) volcanic ash deposition and melting (30); 5) S species/H_2O gas release optimized by high Tharsis altitude; acid precipitation, widespread ice melting (26); 6) local heat pipes (34); 7) shallow contact heating/melting of glacial/cryospheric ice from sill emplacement; 8) catastrophic release of lake water sequestered in VM; 9) dike-assisted groundwater release; 10) rising ELA and PST melting as Mars goes bipolar; 11) cryospheric cracking-assisted groundwater release. All of these mechanisms operate in MAT <<273K.

The Hesperian is characterized by deposition of sulfate deposits (6,35), localized as thick Interior Layered Deposits (ILD) on the floor of VM and in craters in equatorial regions. Abundant fluvial networks and silica-sulfate-rich deposits on the VM rim and flowing into VM (36), are plausibly interpreted to be produced by volcanic ash-induced acid precipitation (26), melting surface snow and ice and draining into VM; activity possibly extends into Amazonian (19).

5) Early Amazonian: VN on Tharsis plateau (Echus, Alba) and Elysium (Hecates) (19) suggest remnant surface ice and continuing effects of volcano-induced acid rains (26); Tharsis still a third pole in EA. Tharsis Montes volcanism transitioning from central edifice to flank eruptions (17), decreasing plinian eruption frequency. Waning OC activity possibly correlative with Vastitas Borealis Formation (VBF) in northern lowlands (37). Global climate period dominated by Anhydrous Ferric Oxide weathering begins (6); minimum surface meltwater alteration implied. First north polar deposits evident (Rupes Tenuis Unit; 37). P_{atm} approaches 100 mbar (Fig. 1).

6) Middle Amazonian: No Tharsis VN or OC; TM volcanism dominantly effusive. V-I interaction produce Elysium lahars (38). North polar region begins accumulating significant layered ice deposits (37). Solar luminosity approaches current value, P_{atm} >~100 mbar (Fig. 1); diurnal amplitude optimum (39) dehydrates any remaining low latitude surface snow and ice. Mars becomes fully bipolar at this time (2-3).

7) Late Amazonian: Mars is fully bipolar with robust polar caps: enters period of dominantly obliquity-driven polar ice mobilization and latitude-dependent (LD) glaciation (40). Surface ice budget largely limited to ~34 m GEL; some removed by non-polar glaciation. MAT and Patm close to that of today. Little to no evidence of top-down melting of glacial ice.

Synthesis: Post-basin M-L Noachian atmosphere largely secondary; Patm likely ~500 mbar, MAT likely <<273 K, water budget low (~2X today's GEL?), ACE produces LN icy highlands, glaciation cold-based, ice thickness <a few 100 m. As atmosphere lost to space, thins from ~500 mbar toward today; Mars starts transition from ADD temperature distribution to today's LDD. Solar luminosity increases from Noachian 75% to today's 100%, increasing equatorial PDT/PST, raising ELA, and enhancing seasonal ablation processes and potential top-down snow-ice melting. LN-EH boundary VN/OBL/CBL form in the icy highlands during a geologically short period; VN recur again in LH-EA in Tharsis, draining into VM to produce sulfates; plinian eruption-induced acid precipitation onto Tharsis snow/ice likely implicated. OCs form over extended time period in H-EA: 11 different viable mechanisms available, all with MAT <<273 K. During Amazonian, decreasing Patm to ~100 mbar causes final decay of ACE; remaining Tharsis cold trap ices migrate to poles and ADD-LDD transition largely complete by Middle Amazonian. LA is bipolar; robust polar ice caps wax and wane due to obliquity variations causing mid-latitude and equatorial glaciation; Mars currently in interglacial (41). In summary, to reach modern Mars P_{atm} (6 mbars) and MAT (213K) from a typical "warm & wet" Noachian Mars, a P_{atm} decrease of 167X the current value, and a MAT decrease of ~67K are required. In contrast, in the scenario outlined here, only modest decrease in Patm (83X) and MAT (~13K) are required. This scenario suggests that some geomorphic indicators of warm/wet climates may be "false positives", and offers multiple predictions and tests to further assess its plausibility.

References: 1. Head et al. 2020, LPSC 51 #2067; 2. Head et al. 2022, LPSC53 #2074; 3. Head et al. 2022, LPSC53 #2083; 4. Fassett & Head 2011, Icarus 211; 5. Melosh & Vickery; 1989, Nature 338; 6. Bibring et al. 2006, Science 212; 7. Palumbo & Head 2017, MAPS 53; 8. Sun & Milliken 2015, JGR 120; 9. Carr & Head 2015, GRL 42; 10. Kite 2019, SSR 215; 11. Wordsworth et al. 2013, Icarus 222; 2015 JGR 120; 12. Head & Marchant 2014, Ant. Sci. 26; 13. Fastook & Head 2015, PSS 106; 14. Scanlon et al. 2018, Icarus 299; 15. Fastook & Head 2023, LPSC 54 #1330; 16. Palumbo et al. 2020, GRL 47; 17. Carr & Head, 2010, EPSL 294; 18. Andrews-Hanna et al. 2010, JGR 115; 19. Fassett & Head 2008, Icarus 195; 20. Fassett & Head 2008, Icarus 198; 21. Goudge et al. 2012, Icarus 219; 22. Buhler et al., 2014, Icarus 241; 23. Morgan et al. 2018, LPSC49 #2219; 24. Hynek et al. 2010, JGR 115; 25. Boatwright & Head 2023, LPSC 54, #1248; 26. Kreslavsky & Head 2020, LPSC 51 #1828; Head et al. 2023, LPSC 54; 27. Cassanelli & Head 2016, Icarus 271; 28. Palumbo et al. 2019, LPSC 50 #2169; 29. Kerber et al., 2015, Icarus 261; 30. Wilson & Head 2007, JVGR 163; 31. Baker et al. 1991, Nature 352; 32. Rotto & Tanaka 1995, USGS Geol. Map; 33. Turbet at al. 2017, Icarus 288; 34. Cassanelli & Head 2016, Icarus 271; 35. Murchie et al. 2009, JGR 114; 36. Mangold et al. 2008, Science 305; 37. Tanaka et al. 2008, Icarus 196; 38. Russell & Head 2003, JGR 108; 39. Fastook et al. 2023, LPSC54; 40. Madeleine et al. 2009, Icarus 203; 41. Head et al. 2003, Nature 426.

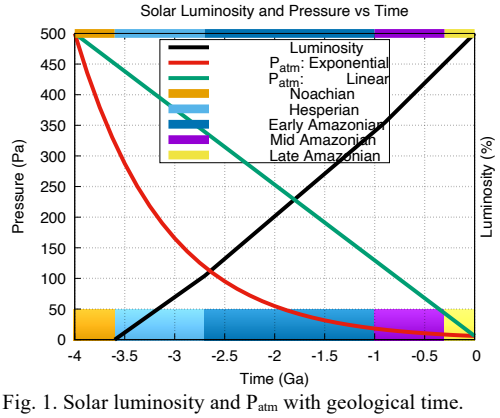

Fig. 1. Solar luminosity and P_{atm} with geological time.